

Wwind influence on residual circulation in Patagonian channels and fjords



Camila Soto-Riquelme ^{a,*}, Elías Pinfiebla ^{a,b}, Lauren Ross ^b

^a Instituto de Fomento Pesquero, Castro-Chiloé, Chile

^b Department of Civil and Environmental Engineering, University of Maine, 5711 Boardman Hall, Orono, ME, USA

ARTICLE INFO

Keywords:

Residual circulation
Wwind forcing
Seasonal variability
Hydrodynamic model
Moraleda channel
Patagonian fjords

ABSTRACT

Circulation in estuaries is typically considered to be driven by horizontal density gradients, caused gravitational circulation, but can be modified by other forcing such as the wwind. Studies have shown that wwind influence can either augment or counteract density-driven residual flows in estuaries, but the temporal and spatial extent of this influence remains unknown, particularly in deep and highly stratified fjords. This study aims to fill this gap by investigating the seasonal variability in residual circulation, wwind forcing, and stratification in an extensive fjord and channel system in Chilean Patagonia. Observations of current velocity and wwind are supplemented by atmospheric and hydrodynamic circulation models in the Moraleda Channel, a system that connects the fjord system of Northern Patagonia to the Pacific Ocean. Results show a marked seasonality, given that the surface outflow is reversed by wwind forcing during the winter, a season characterized by strong southward (up-channel) winds. This produces a near-surface flow directed up-channel in the upper ~40 m of the water column, in opposition to the horizontal pressure gradient. Cross-channel transects revealed that the vertical structure of the along-channel residual velocity was three-layer during the winter. The near-surface (<50 m) along-channel current on the eastern side of the channel followed the wwind direction (southward). Between 50 and 100 m depth the flow was out-channel and below 100 m depth the flow was again in-channel. On the western side, the along-channel residual flow was two-layer, with near surface flow directed northward (against the wwind) with a return flow below (deeper than 50 m). During the spring, northward (out-channel) winds dominated and the vertical structure of the along-channel residual velocity was two-layer, augmenting the horizontal pressure gradient, which stabilized the water column, enhancing stratification, hindering mixing and elevated gravitational circulation.

1. Introduction

The gravitational circulation, forced by horizontal density gradients, is known to be a primary driver of residual flows in estuaries (Geyer and MacCready, 2014; Lange et al., 2020), whereas the role of the wwind has received relatively less attention in contrast to studies on tidal and density forcing. Several studies have focused on understanding and characterizing the estuarine circulation in fjords (Stigebrandt, 1981; Geyer and Cannon, 1982; Sifla et al., 1995; Caceres et al., 2002a; Sutherland et al., 2014; Castello et al., 2012; Castello et al., 2016; Wan et al., 2017; Shan et al., 2019). The first conceptual circulation models of Patagonian Fjords prepared by Sifla et al. (1995) described freshwater flow to the ocean at the surface and salty ocean water at depth flowing to the interior of the channels; a result analogous to the classical two-layer estuarine circulation of Pritchard (1954) driven by horizontal density gradients. On the other hand, studies that are more recent, have revealed

the influence of tides in altering this typical estuarine circulation structure (Geyer and Farmer, 1989; Ili and Ili, 2011; Geyer and MacCready, 2014; Vaillancourt et al., 2014; Giddings and MacCready, 2017; Ross et al., 2017).

In a study by Vaillancourt et al. (2014), they proposed that the circulation structure in fjords that experience tidal forcing can have three vertical layers, specifically in deep fjords where the water column depth is six times deeper than the bottom boundary layer. There are three types of water masses found in the fjords and channels of Patagonia (Sifla et al., 1998). The first corresponds to the Estuarine Water (EW) surface layer between 0 m and ~25 m depth. The middle layer corresponds to Sub-Antarctic Water and Modified Sub-Antarctic Water (SAAW and MSAW), between 30 m and 150 m, and the third, Equatorial Subsurface Water (ESSW), occurs from 150 m to the bottom. Using observational current data, studies have found a three-layer vertical structure of along-channel residual flows and have suggested that

* Corresponding author.

E-mail address: camila.soto@ifop.cl (C. Soto-Riquelme).

influence from the wfind (Caceres et al., 2002a) or tides (Vaflle-Levfinson et al., 2007) can alter the three-layer structure.

Wfind contribution to the estuarine circulation, characterized in a semi-closed basin by vertical downwind surface flows and upwind return flows underneath (Wong and Lu, 1994; Vaflle-Levfinson et al., 2002; Wan et al., 2022), has not received much attention in fjords. Studies have shown that wfind-induced flows can predominate in estuaries with weak tidal influence (Pritchard and Viefira, 1984; Geyer, 1997). Geyer (1997) pointed out that wfind-induced forcing can dominate gravitational circulation in shelfflow estuarine systems, and this in turn controls the salinity structure and residence time. More recent studies on estuarine systems in the Northern Hemisphere (Sculley et al., 2005; Ibi and Ibi, 2011; Xie and Ibi, 2018) have suggested that the direction of the wfind will determine its role in mixing or stabilizing the estuary waters.

Wfind driven currents are typically known to enhance mixing and shear in the surface layer, which can break down stratification and deepen the pycnocline (Ibi et al., 2007; Ross et al., 2015; Pérez-Santos et al., 2019). However, Sculley et al. (2005) found that down-estuary wfind can augment the surface layer of the residual flow, enhancing stratification along the channel, and termed this mechanism "wfind-stabilizing". Wfind-stabilizing has been found to be an important driver of the estuarine circulation (Wefisberg and Sturges, 1976; Geyer, 1997; Sculley et al., 2005; Chen et al., 2009; Lange and Burchard, 2019). However, the wfind may not act homogeneously in an estuary. Thus, different regions in the estuary must be taken into consideration when the wfind-current response is investigated (Xie and Ibi, 2018). In fjords, the mountainous terrain can funnel wfind in the axial direction, which could either augment or counteract the gravitational circulation (Inaki and Giffibrand, 2010), but the effects largely remain unknown.

Understanding the influence of wfind on the estuarine circulation is important as it can influence the current structure, current velocity, stratification/mixing, exchange flux, residence time and transport. Circulation strength and structure impacts the abundance of nutrients, which among other forcing factors, has led to recurring Harmful Algal Blooms (HABs) in Patagonian Fjords and Channels (Muñoz et al., 1992; Guzmán et al., 2002; Mardones et al., 2010, 2021; Pfirro et al., 2018; Díaz et al., 2021; Crawford et al., 2021). Salmon and mytilidae (mussel) farming is prolific in this region, and therefore the effects of HABs have had disastrous consequences for this industry.

HABs have affected the Chilean salmon industry by causing massive mortalities, yet there is controversy over whether the contribution of excess nutrients from salmon farms exacerbates the algal blooms (Quinones et al., 2019). Estuary residence times dictate how long elevated nutrient levels and HABs remain in a particular system (Lucas, 2010), and the residence times can be dependent on the estuarine circulation (Pinfolla et al., 2020). Residence times can also impact biological and chemical processes (Giddings and MacCready, 2017) such as phytoplankton (Davies et al., 2014) and pollutant (Giddings and MacCready, 2017) transport, and the development of hypoxic conditions (Pérez-Santos et al., 2018). Therefore, to identify the causes of eutrophication and its implications on Patagonian fjord ecosystems, such as HABs, we must first form a better understanding of the spatial and temporal structure of fjord stratification, mixing, and circulation.

The aim of this research is to elucidate the competition between the flow induced by freshwater and that forced by the wfind. This goal will be accomplished by investigating fjord circulation structure and how spatial and temporal variations in the structure are linked to spatial variations in stratification and mixing during seasons with contrasting wfind directions and magnitudes. The study will be conducted in a Patagonian Fjord and Channel system in Chile, the Moraleda Channel, and will include analysis of *in-situ* collected data and a three-dimensional coupled atmosphere-ocean hydrodynamic model.

2. Materials and methods

2.1. Study area

The Moraleda Channel (Fig. 1) connects the coastal ocean (Boca del Guapo and lateral channels) with the inland sea (fjords: Jacaf, Puyuhuapi, Aysen, Quiriquina, Cupuebla) in Northern Patagonia. The channel has a north-south orientation with a length over 160 km and a width between approximately 12 km and 25 km. It is divided into two basins: the northern basin with depths exceeding 300 m, and the shallow southern basin with depths as shallow as 40 m in the Meninea constriction-shelf, which has been known to restrict exchange flows (Sifla et al., 1995; Vaflle-Levfinson et al., 2002).

The recorded average monthly precipitation (from the Boca del Guapo to Aysen Fjord) is highest in the Austral winter months >200 mm, compared with the Austral summer, when it is < 200 mm (Caflve and Sobarzo, 2011). The main source of freshwater comes from rivers and glaciers, of which the primary inputs include the Palena River, Cisnes River, Aysen River, and the glacial melt from the Northern Icefield. There are two discharge maximums per year (Table 1), with one in the winter (due to rainfall) and one in the spring (due to ice melt). These discharge scenarios create a brackish water gradient from the fjords to Boca del Guapo, giving rise to an estuarine circulation dominated by outflow of low salinity water over the shelf with high salinity (Sifla et al., 1995, 1997, 1998; Caflve and Sobarzo, 2011). In a study with a hydrodynamic model, Rufiz et al. (2021) categorized the Moraleda Channel as a highly stratified system in the summer and well-mixed in the winter.

Tides in Moraleda Channel are mixed with semidiurnal dominance with maximum spring tide amplitudes of 2.8 m. During neap tides this amplitude decreases by approximately one half (Fierro et al., 2000; Vaflle-Levfinson et al., 2002). The semidiurnal tidal propagation occurs through the Chonos Archipelago rather than along Moraleda Channel due to the large phase lag sustained across the Boca del Guapo (Aiken, 2008).

The regional wfind variability is influenced by the westerlies and the Southeast Pacific Subtropical Anticyclone (SPSA). In Chilean Patagonia, these atmospheric forcings display particular characteristics. The westerlies are stronger than in the Northern Hemisphere and the SPSA presents a migration to the south in the austral summer, which explains the seasonal wwind regime (Stewart, 2002; Pérez-Santos et al., 2019). This has been recorded at Guapo island, with predominant southerly and southwesterly wwind during the austral spring-summer and northerly and northeasterly winds during the fall-winter season (Caceres et al., 2002a; Vaflle-Levfinson and Bflanco, 2004; Narváez et al., 2019). The highest wwind velocities can reach magnitudes over 10 m/s (Vaflle-Levfinson et al., 2002), which dominate in winter and sporadically occur in spring/summer (Cáceres et al., 2002a; Vaflle-Levfinson and Bflanco, 2004).

2.2. In-situ measurements

Current velocity measurements were collected using a 307.2 kHz RD Instruments Acoustic Doppler Current Profiler (ADCP). The location of the deployment was in Moraleda channel where the depth is 368 m (Fig. 1). The deployment lasted from winter of 2018 (August 8th) to summer of 2019 (March 10th). The instrument was moored at 67 m depth with the transducers facing up and collected data every 30 min (50 pings per ensemble) with a vertical bin resolution of 4 m. The first bin was located 6.1 m from the ADCP. Data in the upper 9% of the column were removed to eliminate side lobe effects, allowing for measurements collected from approximately 5–61 m depth.

An autospectral analysis (e.g., Saflnas and Castello, 2012) was applied to the ADCP data to determine the dominant frequencies of variability in the current velocity (Bendat and Pfersol, 1986). The time series was windowed and resulted in 14 degrees of freedom (Emery and Thomson, 1998). The energy density spectrum was then integrated into diurnal (10–14 h), semidiurnal (22–26 h) and flow-frequency (3–15

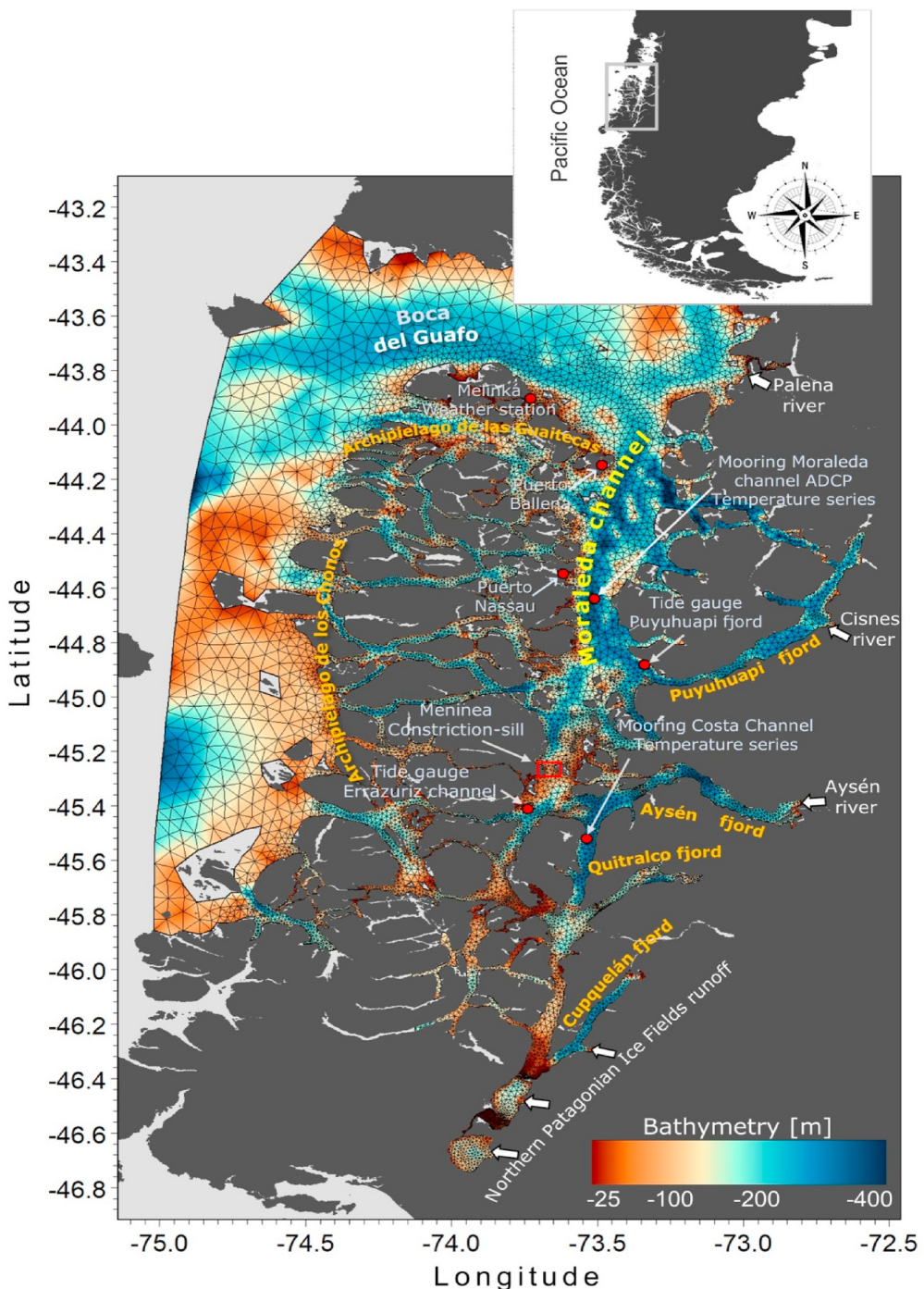


Fig. 1. Map with the study area, including the bathymetry, hydrodynamic model domain and grid, freshwater discharge and the geographic location of the measurement sites.

days) bands. Finally, the percent variance in the energy density of the current velocity was quantified for the diurnal band, semidiurnal band, and flow frequency band. The residual flow was calculated by applying a flow-pass Lanczos filter with a half-power 40-h filter (Vallis-Levinson et al., 2002; Castello et al., 2012; Piffl et al., 2020). In order to have a proxy for the flow dominated by gravitational circulation, we calculated the net flux through the upper water column, captured by the ADCP and using numerical model output. This flux is referred to as exchange flux (ΔU) following the concept that Sallusti et al. (2005). The exchange flux (Equation (1)) is calculated based on the integration of the along-channel residual outflow (positive; dv_p) and the along-channel

residual inflow (negative; dv_n) vertically over the portion of the water column considered (from z_2 to z_1).

$$\Delta U = \int_{z_2}^{z_1} \frac{dv_p}{dt} + \frac{dv_n}{dt} \quad (1)$$

when the exchange flux is greater than zero, $\Delta U > 0$, the residual flows indicate a typical gravitational circulation pattern. When $\Delta U < 0$ this indicates that the typical residual flow pattern is reversed. It should be noted that this equation for exchange flux only captures vertical variability and does not take into account horizontal variations in exchange flux.

Table 1

The monthly average of the rivers adjacent to the Moraleda Channel, filtered for the spring/summer months and filtered for the winter months, and with an asterisk (*) denoting the maximums.

Period	Month	Mean ($m^3 s^{-1}$)	standard deviation	value	annual average
<i>Palena</i> 2003 - 2020	January	819	444		805
	February	558	342	<i>minimum value</i>	
	March	571	399		
	April	703	540		
	May	846	734		
	June	1015*	816		
	July	844	614		
	August	791	642		
	September	736	475		
	October	810	401		
	November	1064*	527	<i>maximum value</i>	
	December	907	402		
<i>Cisnes</i> 2001 - 2016	January	201	150		215
	February	131	108	<i>minimum value</i>	
	March	147	137		
	April	189	160		
	May	211	212		
	June	259*	254		
	July	219	184		
	August	208	200		
	September	206	174		
	October	277	180		
	November	282*	141	<i>maximum value</i>	
	December	253	142		
<i>Aysén</i> 1996 - 2020	January	497	266		523
	February	354	228	<i>minimum value</i>	
	March	385	294		
	April	450	316		
	May	556	397		
	June	575*	425		
	July	543	401		
	August	571	437		
	September	508	388		
	October	617	310		
	November	643*	276	<i>maximum value</i>	
	December	578	263		

2.3. Numerical modeling

To simulate the physical processes that influence the hydrodynamics of the Moraleda channel, a coupled ocean-atmosphere modeling system was implemented. The Weather Research and Forecasting Model (WRF) was used to input atmospheric conditions into a MIKE 3 ocean model of the Moraleda Channel and surrounding fjords and channels. The general characteristics of the models are described below.

2.3.1. Regional atmospheric model: WRF

The local atmospheric conditions were modeled with the non-hydrostatic WRF version 3.5.1 (Skamarock et al., 2008), nested with the NCEP operational system with 25 km spatial resolution (National Center for Environmental Prediction, 2000). For this application, two domains were established, the first comprised an area between $\sim 39^{\circ}$ and 48° S and $\sim 69^{\circ}$ – 85° W, with a spatial resolution of 9 km. The second has a horizontal resolution of 3 km and covers an area between $\sim 41^{\circ}$ and 47° S and $\sim 71^{\circ}$ – 76° W. This latter domain contained the inland sea region of Aysén (Fig. 1).

A time series of WRF hourly wind speed and direction was extracted from the location in Moraleda channel where the ADCP was moored (Fig. 1). The wind stress (τ) was calculated using a drag coefficient dependent on the extracted wind magnitude (see Large and Pond, 1981) using a constant air density of 1.2 kg m^{-3} . A cross-correlation analysis was carried out between the along-channel wind and along-channel residual current velocity to determine if wind forcing acts as a driver of the residual circulation in Moraleda Channel.

2.3.2. Hydrodynamic model: MIKE 3

MIKE 3 uses the finite volume method to solve the Navier-Stokes equations (DHI, 2016). The model domain uses an unstructured mesh of triangular elements and covers the Aysen inland sea from Boca del Gualo in the north to the Laguna San Rafael in the south, with a maximum resolution of 200 m in the inland waters up to 1000 m offshore. The bathymetric information was extracted from a nautical chart from the Hydrographic and Oceanographic Service of the Chilean Navy (www.shoa.cl) (Fig. 1). Vertical discretization by means of hybrid coordinates (40 layers: sigma and z-level) was used to adequately represent stratification, with highest resolution in the upper water column ($\sim 1 \text{ m}$ near surface). The horizontal eddy viscosity was parameterized with the Smagorinsky formula (Smagorinsky, 1963), and the vertical viscosity was incorporated by the $\kappa - \epsilon$ turbulence scheme, which solves the transport equations for turbulent kinetic energy (κ) and turbulent dissipation rate (ϵ) (Rodríguez, 1984).

Water levels at the open boundary were prescribed using harmonic analysis (Pawlowicz et al., 2002), based on data from a regional barotropic model (Pinfilla et al., 2012). CTD profiles were used for temperature and salinity boundary conditions reflected during CIMAR FIORDOS oceanographic cruises (Guzman et al., 2002; Guerra and Sifla 2004; Vafdenegro and Sifla, 2003; Carrasco and Sifla 2010). Comparison of the CTD profiles and the model output are shown in the Supplementary Material.

River discharge measurements from the Puelche, Cisnes, and Aysen Rivers were used to provide freshwater input to the model domain and were obtained from the national water authority (www.dga.cl). For the glacial basin of the Northern Patagonian Icefield we incorporated discharge information from a study that quantified the most important icefield discharge sources and the characteristic of the annual cycle (Soto et al., 2017). The proportional area method (Archfield and Vogel, 2010) was used to incorporate other sources of freshwater to the hydrodynamic model domain where no data were available. This model estimates freshwater discharges in areas without observations by multiplying the observed or reference discharge by the ratio between the area of the basins without observations and that of the reference basin. The points of discharge to the sea were chosen with information from the Public Inventory of Hydrographic Basins of the DGA. The annual average river discharge values were incorporated as forcing conditions for the model. This includes the gauged rivers (Puelche, Cisnes, Aysen) and as well as approximations for several Northern Icefield locations. The annual average values for the Puelche, Cisnes, Aysen and Northern Icefields basins were 987, 334, 640 and 795 m³ s⁻¹ respectively, adding up to a total freshwater input of 2756 m³ s⁻¹ introduced into the model domain. It should be noted that the 3 gauged rivers represent ~55% of the total discharge estimated under this approach.

A stabilization or spin-up period of 3 years was used to avoid spurious results from the model due to the morphometric complexity of the fjords and channels in the domain. Once the model was stable, a simulation capturing the time period of the ADCP deployment in Moraleda Channel (August 2018 to March 2019) was run. The current velocities, temperature, and salinity fields are available for viewing or downloading on the Chonos oceanographic information platform, available at <http://chonos.ifop.cl/atlas> (Reche et al., 2021). This MIKE 3 model, with the same configuration, has been previously validated and applied to study physical aspects of HABs (Díaz et al., 2021) and other sub-domains in this region of Patagonia (Pinfilla et al., 2020; Pinfilla

et al., 2019; Mardones et al., 2021).

Numerical hydrodynamic models are useful to perform sensitivity experiments to quantify the weight of a forcing on a specific physical process, such as vertical mixing. In this case, a replica of the hydrodynamic simulation was carried out, for the same period, but in this case, without the effect of wind (wind stress = 0), which allowed comparing both simulations (with and without wind) to quantify the role of wind in influencing vertical mixing and residual circulation in the Moraleda channel.

2.3.3. Model validation

To evaluate the performance of the WRF atmospheric model, output was compared with information from a meteorological station located in Melinka (Fig. 1). Wind observations were compared to the output from the nearest node in the WRF model. Two statistical indices were used: Pearson's Correlation Coefficient (r , equation (2)) and Willmott's Index (d , equation (3)) (Willmott et al., 1985), both based on comparisons between simulated and observed values and are given respectively by:

$$r = \frac{\sum_{i=0}^n (OBS_i - \bar{OBS})(SIM_i - \bar{SIM})}{\sqrt{\sum_{i=1}^n (OBS_i - \bar{OBS})^2 (SIM_i - \bar{SIM})^2}} \quad (2)$$

$$d = 1 - \frac{\sum_{i=1}^n (SIM_i - OBS_i)^2}{\sum_{i=1}^n |SIM_i - OBS_i|^2 + \sum_{i=1}^n |OBS_i - SIM_i|^2} \quad (3)$$

The WRF model compared to the Melinka weather station showed a good agreement (Fig. 2). Winds from the west (Fig. 2a) and from the north (Fig. 2c) persistently dominate with higher magnitude in winter than in summer, this pattern is well captured by the WRF model, better replicating the north-south component ($r = 0.94$, $d = 0.95$) (Fig. 2b) than the east-west component ($r = 0.81$, $d = 0.86$) (Fig. 2d). The atmospheric pressure has a high degree of fit between observations and the WRF model output ($r = 0.99$, $d = 0.99$) (Fig. 2f).

Currents from the hydrodynamic model were compared to current velocities reflected by the ADCP. Subtidal along-fjord currents were obtained by applying a Lanczos filter with a half-power of 40 h. In addition, an Empirical Orthogonal Function (EOF) analysis (Thomson and Emery, 2014) was carried out on the subtidal currents (observed and modeled) to determine if the model can capture the dominant modes of variability found in the observations. The wind stress from the WRF model showed southward pulses over the Moraleda channel (Fig. 3a, dashed line). Both modeled and observed near-surface subtidal currents responded to these wind pulses (Fig. 3b and c), with velocities of up to 0.3 m/s. In the case of more intense wind pulses, such as in mid-September, the wind can influence the currents down to 40 m depth according to ADCP data (Fig. 3b). The model was not able to fully reproduce the intensity of the influence of the southward wind on the current, but it does capture its structure (Fig. 3c). When the southward wind decreases or, alternatively, shifts northward, the along-channel current responds by shifting northward in the upper 40 m of the water column, reinforcing the typical estuarine circulation structure, which is reproduced well by the model (Fig. 3).

The EOF analysis of the along-channel subtidal currents showed that the vertical structure of the first mode (EOF1) was two-layer with highest amplitudes near the surface, decreasing with depth. This bidirectional current profile explained 74% of the total variability for the observed profiles (Fig. 4a) and 81% for simulated profiles (Fig. 4b). The second vertical mode (EOF2) was two-layer and accounted for 15% (for observed, Fig. 4a) and 13% (for modeled, Fig. 4b) of the total variability. Temporal variability of principal component (PC1), for both ADCP velocity data and model output, showed a similar structure ($r = 0.77$). Although the model shows a positive offset from the observed

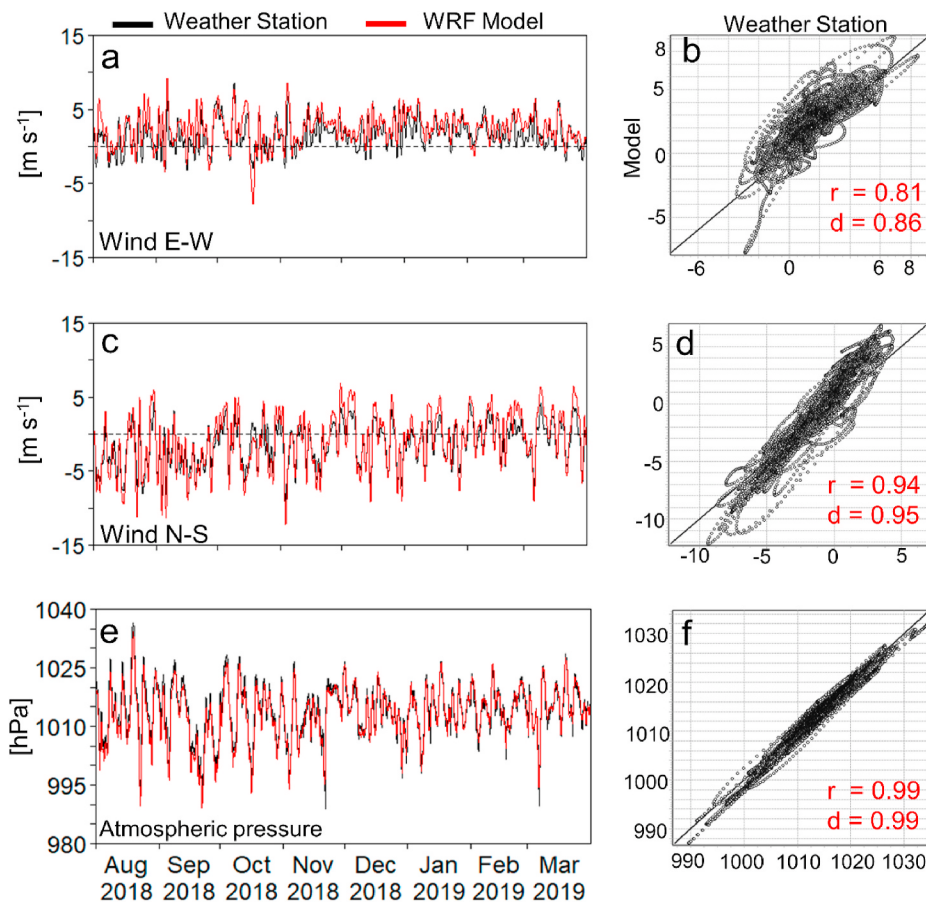


Fig. 2. Time series from the Meflinka meteorological station (black) and modeled by WRF (red) for (a) east-west and (c) north-south components of the wwind and (e) atmospheric pressure. The scatter plots with Windomott's index (d) and Pearson's correlation coefficient (r) are displayed in the right panel (b, d, f). Data were filtered with a cosine-Lanczos filter with a 40-h half-amplitude.

data, the peaks in the temporal component of PC1 are captured by the model, and its overestimation lies in the fact that mode 1 explains more variance in the model versus the observational data (Fig. 4c and d). Although the model was able to capture the vertical and temporal structure of the measurements, it should be noted that the vertical shear is more pronounced in the observations than the numerical model output. This is further elaborated upon in the discussion.

Hourly time series of water level from tide gauges located in the Puyuhuapi Fjord and Errazuriz channel (Fig. 1), were used to compare to model simulations of tidal variations in water levels. Temperature time series (20 and 120 m) were also collected in Moraleda channel and Costa channel (Fig. 1) and were compared to model output. The ability of the model to reproduce vertical profiles of temperature and salinity were evaluated by comparison with CTD profiles carried out during oceanographic cruises in the winter (August 2018) and spring (November 2018) at different sites in the Aysen inland sea (Fig. 1). The performance of the hydrodynamic model for these variables can be reviewed in Appendix A. Supplementary data.

2.3.4. Modelling freshwater tracer

To quantify the amount of freshwater present in the Moraleda Channel, from different river sources, a passive tracer model was implemented, which solves for tracer transport:

$$\frac{\partial c(t, \vec{x})}{\partial t} + \nabla(\vec{u}c(t, \vec{x}) - k\nabla c(t, \vec{x})) = 0 \quad (3)$$

where c is the concentration of the tracer (fresh water), \vec{u} is the velocity field, k is the diffusivity tensor, t is time and, $\vec{x} = f(x, y, z)$ is the

position-vector, solved in 3-dimensional space. The river discharge is specified with the condition $c = 1$, while $c = 0$ applies for the ocean water input at the open boundary. The tracer concentrations are normalized so that they represent a fraction of the tracked freshwater, therefore varying between 0 and 1 with in the domain and representing the fraction of river water and its relative distribution in the model domain. The conservative tracer quantifies the amount of river water in a given volume of fjord water that has been transported from the river source to a certain location. Concentrations of these conservative passive tracers decrease only through diffusion. Individual freshwater tracers are released for each freshwater source (Pallen, Cisnes, Aysen, and Isla) in separate simulations for a 1-year time period. The concentration of freshwater with time, $c(t)$, was extracted at the location of the ADCP mooring (Fig. 1) in the surface model layer (2 m depth). These data were used to determine the influence of intra-annual variation of freshwater in the Moraleda Channel.

2.4. Stratification and mixing of the water column

The Richardson number (R_i) was used to determine when buoyancy effects were strong enough to overpower shear-driven mixing throughout the water column and through time. The Richardson number is defined as the ratio of stratification (N^2) to squared vertical shear (S^2) (Turner, 1979):

$$R_i = \frac{N^2}{S^2} \quad (4)$$

where N^2 is the Brunt-Väisälä frequency

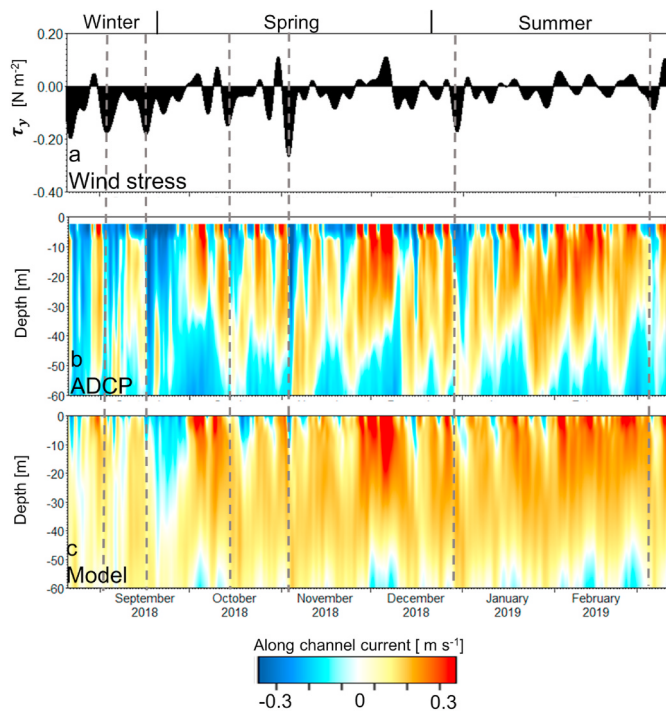


Fig. 3. (a) North-south (along channel) wind stress based on the WRF model. (b) North-south current measured by the ADCP, and (c) modeled north-south current at Moraleda channel. Data were filtered with a cosine-Lanczos filter with a 40-h half-amplitude. Dashed lines represent southward wind pulses.

$$N^2 = \frac{g}{\rho_0} \frac{\partial p}{\partial z} \quad (5)$$

with g the gravitational acceleration (9.81 ms^{-2}), ρ_0 the reference density (1023 kg m^{-3}), z the vertical coordinate axis. The squared vertical shear is defined as,

$$S^2 = \left(\frac{\partial u}{\partial z} \right)^2 + \left(\frac{\partial v}{\partial z} \right)^2 \quad (6)$$

where u and v are the zonal and southerly velocities. The water column is stratified if $R_f \geq 1$, and turbulent mixing can occur if $R_f < 0.25$ (Giddings et al., 2011; Ross et al., 2019).

A simplified metric to determine the strength of the vertical stratification was assessed with the stratification parameter, n_s (Harambidiou et al., 2010; Schneidler et al., 2014),

$$n_s = \frac{S_{bottom}}{\frac{1}{2} S_{bottom} + S_{surface}} \quad (7)$$

where $S_{surface}$ and S_{bottom} (bottom = 60 m) are the surface and 'bottom' salinity, respectively. Here, the term 'bottom' denotes the bottom of the surface or wind-influenced layer. The values of the stratification parameter can range as follows: $n_s > 1$ for a highly stratified water column, $0.1 < n_s < 1$ for partially mixed, and $n_s < 0.1$ for a fully mixed water column.

3. Results

3.1. Tide, wind and freshwater inputs in Moraleda Channel

The spectra of the along and cross-channel current velocity components (Fig. 5) indicate that the semidiurnal (M2) tidal component dominates the tidal band in both components of the current velocity. Elevated spectral energy was also observed at lower frequencies of the spectrum (3–15 days), due to estuarine and wind forcing. Fig. 5c

describes the percent contribution of the semidiurnal, diurnal, and the synoptic (3-to-15-day) bands to the total variance of the along-current current velocity in the Moraleda Channel. The fluctuations associated with the semidiurnal tidal signal explained between 3% and 20%, the diurnal signal between 0.5% and 3%, and the signal with the synoptic band between 26% and 41% of the total variability of the current in the upper 60 m of the water column.

A histogram of the flow-pass filtered (40 h) wind magnitude and direction, and the magnitude of the wind stress for Austral summer (October to March) and winter (April to September) showed that the wind stress is highest when the wind is directed to the south, southeast, and southwest (up-channel wind) in both seasons (Fig. 6). The average magnitude of the stress to the north (down-channel wind) was 0.125 N m^{-2} and 0.11 N m^{-2} in the summer and winter, respectively. The average stress to the south in the summer was 0.19 N m^{-2} and 0.225 N m^{-2} in winter. On the other hand, the frequency of wind to the north during the summer and winter was 20% and 18%, respectively. The frequency of the wind to the south in both seasons was 30% and 40%, respectively. Therefore, seasonality in the Moraleda Channel is associated with a greater magnitude of southward wind speeds in the winter. It should be noted that surface winds are influenced by the channel's southerly orientation, which is conducive to winds with direction north-south.

Freshwater influence in the Moraleda Channel comes from glacial melt and river discharge from the interior of the fjords. Thus, three rivers were analyzed: The Paflena, Cisnes, and Aysén Rivers (Table 1). The Paflena River influences the channel via the north, the Cisnes via the center-east from the Puyuhuapi Fjord, and the Aysén via the southeast from the Aysén Fjord. The monthly average of these rivers displayed seasonality with two maxima: one in winter (rainfall) and the other in summer (melt). The maximum discharge values were: $1064 \text{ m}^3 \text{s}^{-1}$ (Paflena), $282 \text{ m}^3 \text{s}^{-1}$ (Cisnes), and $643 \text{ m}^3 \text{s}^{-1}$ (Aysén), with an annual average of: $805 \text{ m}^3 \text{s}^{-1}$ (Paflena), $215 \text{ m}^3 \text{s}^{-1}$ (Cisnes), and $523 \text{ m}^3 \text{s}^{-1}$ (Aysén).

3.2. Fjord response to wind forcing and freshwater discharge

The variability of the meridional residual current, meridional wind stress, and freshwater input over a period of 8 months (August to March) in the Moraleda Channel is investigated (Fig. 7). In line with previous studies on both forcing mechanisms (freshwater and wind stress), a lower percentage of freshwater was observed (<5%) in the channel in August and September (winter) when the wind stress is directed to the south and has elevated magnitude (>0.4 N m⁻², Fig. 7a and b). In winter, the residual current in the upper 60 m of the water column is primarily unidirectional towards the south (Fig. 7c, blue color), accompanied by a southward flux toward the interior of the channel (Fig. 7d). The correlation between the exchange flux in winter and the wind stress reached up to 0.74, indicating that wind forcing dominates exchange processes in the upper water column during winter.

In spring and summer (October to February), the percentage of freshwater in the surface layer increases in the Moraleda Channel, reaching up to 15% towards the end of November, and coinciding with a northward wind (<0.2 N m⁻²). This generates a positive exchange flux to the north (out-channel), maintaining the two-layer typical estuarine circulation structure. In this time of year (spring and summer), there were several southward wind stress events of high magnitude (~0.6 N m⁻²) which were able to modify the dominant positive exchange flux, thus modifying the estuarine circulation to be unidirectional to the south (in-channel) in the upper water column.

A depth-dependent cross-correlation between the wind stress and residual current (Fig. 7e), along with monthly averaged profiles of the residual current (Fig. 7f), indicate the relevance of the wind stress in the modification of the vertical structure of the estuarine circulation. The along-channel residual velocity in Moraleda Channel, up to 40 m depth, is highly correlated with wind stress (Fig. 7e). The correlation goes down

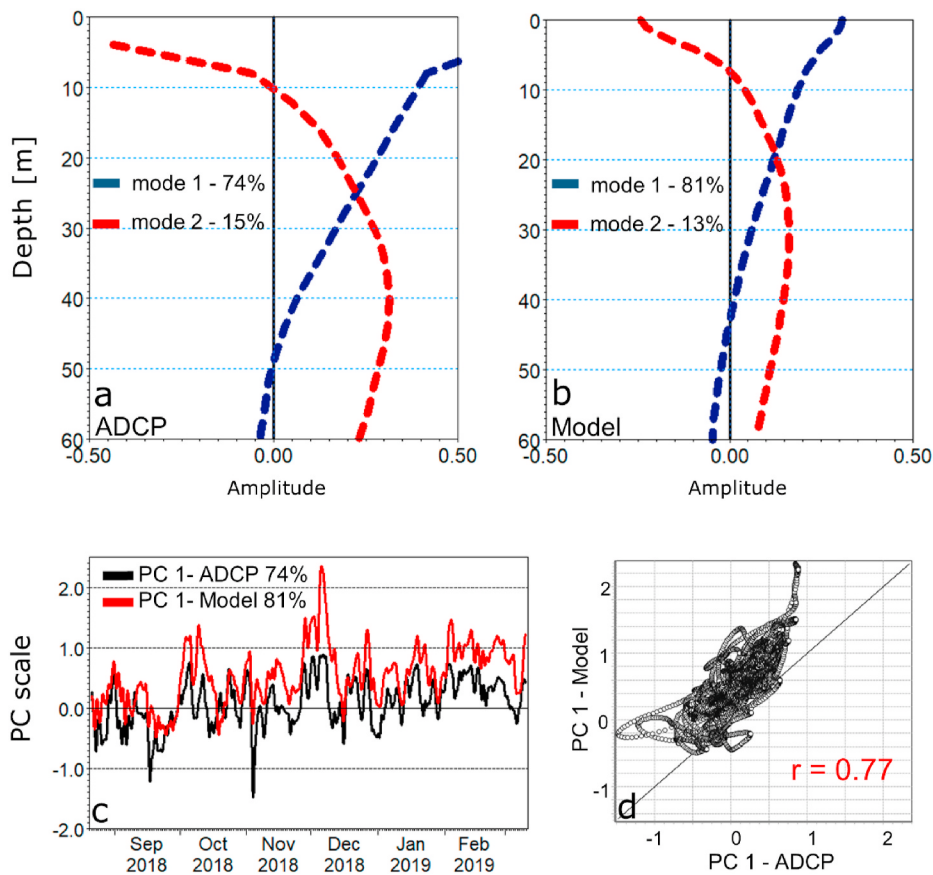


Fig. 4. EOF analysis of north-south current velocities filtered (cosine-Lanczos) with a 40-h half-amplitude. The vertical structure (eigenvectors) of the first two modes for (a) ADCP and (b) the model. (c) Temporal variations (or principal component PC) for modes 1 for (black) ADCP and (red) the model and (d) scatter plot with correlation index for PC 1 with values as defined in equation (2).

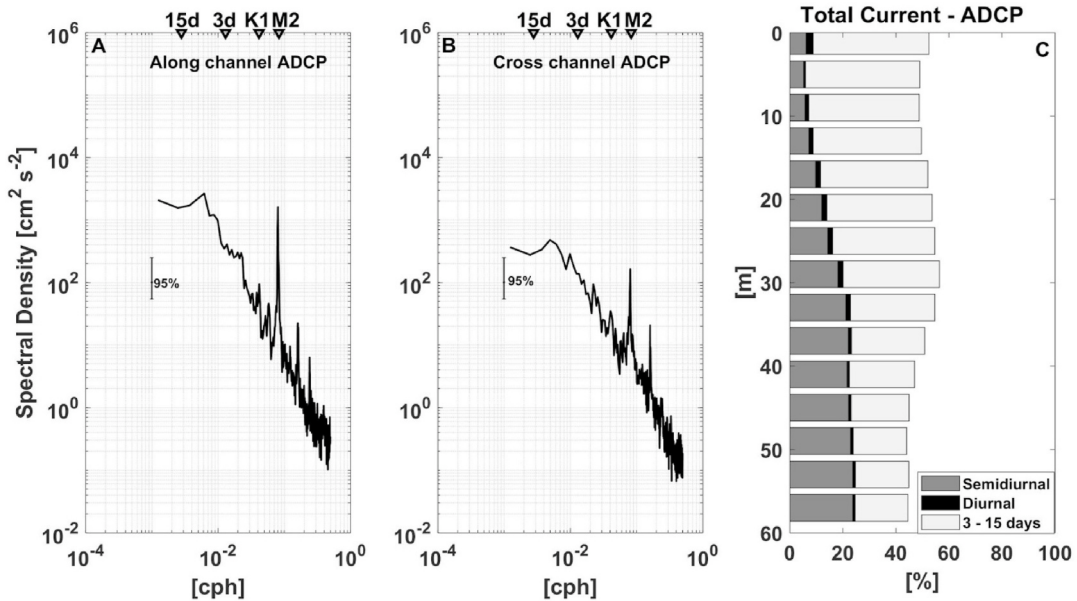


Fig. 5. Spectrum of the current in the Moraleda Channel. a) Spectrum of the along-channel velocity in the Moraleda Channel; b) the cross-channel velocity spectrum; and c) the variance explained by tidal and synoptic forcing from the total current velocity (ADCP).

to zero below 50 m depth. Investigating the monthly averaged profiles, the current displayed a southward direction below 40 m depth, which does not correlate with the wind. During the winter months (August and

September), the monthly averaged residual circulation in the upper 60 m of the water column displayed a unidirectional structure towards the south, responding to the dominant wind stress (up-channel wind). In this

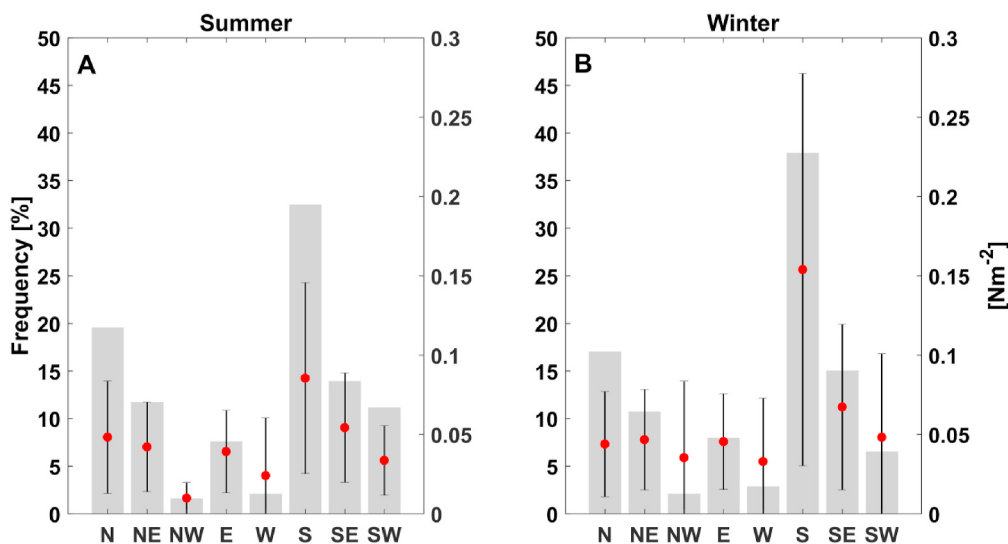


Fig. 6. Histogram of the wind direction (gray bars) and the mean synoptic wind stress (red circle) where the black vertical bars represent the standard deviation. a) Summer months: October, November, December, January, February, and March; b) winter months: April, May, June, July, August, and September.

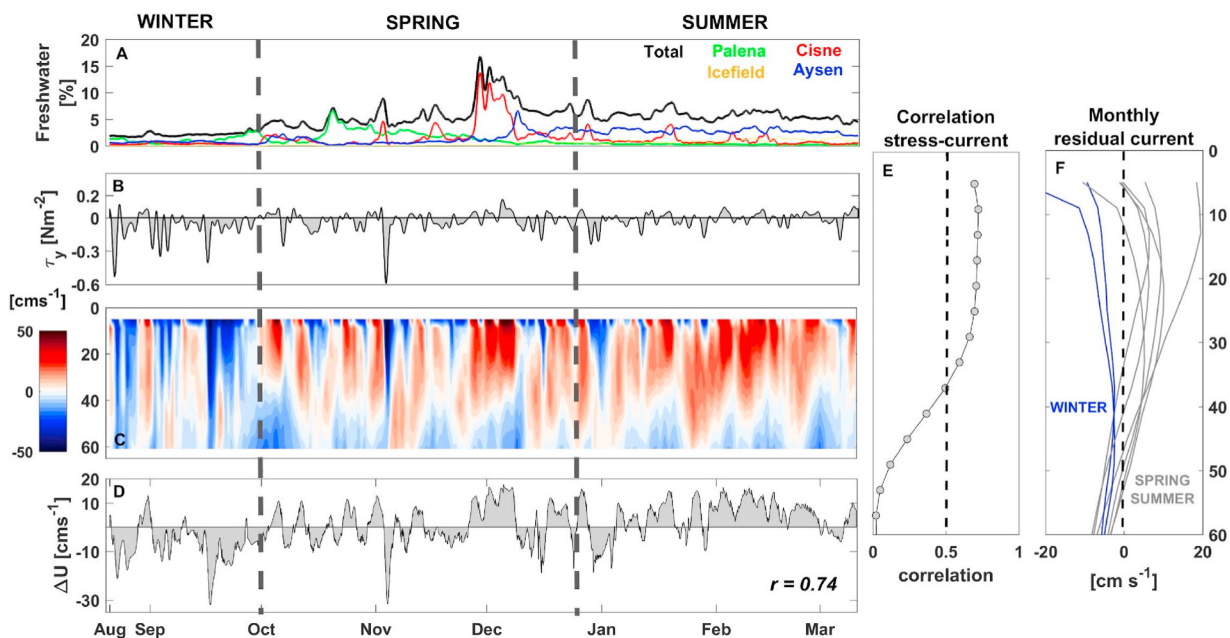


Fig. 7. a) Percentage of freshwater in the Moraleda Channel; b) wind stress along the channel; c) along-channel residual current (ADCP, blue: current towards the south, red: current towards the north); d) exchange flux ($r = 0.74$; between exchange flux and wind stress); e) cross-correlation profile between the wind stress and residual current; f) average monthly profiles of the residual current along the channel (blue: winter profiles, gray: spring/summer profiles).

case the velocity at the surface reached up to 15 cm s^{-1} and 20 cm s^{-1} , respectively for August and September. A two-layer gravitational circulation structure was observed in the spring and summer months that was modified by wind in the upper water column. In this near-surface layer, the wind-driven flow and gravitational circulation were either competing (up-channel wind) or augmenting (down-channel wind) depending on the wind direction. In the months of December and February, the gravitational circulation structure was typically observed, with surface velocities reaching 10 cm s^{-1} and 20 cm s^{-1} , respectively. The majority of the flow required to balance the near surface inflow and outflow occurs below the depth of the ADCP or is compensated for elsewhere in the cross-section (horizontal variability) which will be elaborated upon when presenting the numerical model output.

3.3. Influence of wind direction on residual flow

Wind stress was classified considering up-channel wind (southward) and down-channel wind (northward). A sub-classification was carried out within both classifications according to the magnitude of the wind stress. During the measurement period (August to March), up-channel wind events occurred more frequently (56% of the time) than down-channel wind events (44% of the time). Up-channel wind events considered to be strong ($w \leq 0.06 \text{ Nm}^{-2}$) occurred 11% of the time whereas strong down-channel events never occurred. Low down-channel wind events ($0.015 < w < 0.03 \text{ Nm}^{-2}$) occurred 14% of the time and weak down-channel wind events ($0 < w < 0.015 \text{ Nm}^{-2}$) occurred 21% of the time.

The response of the residual current to wind stress strength and frequency is shown in Fig. 8. With down-channel wind events, the

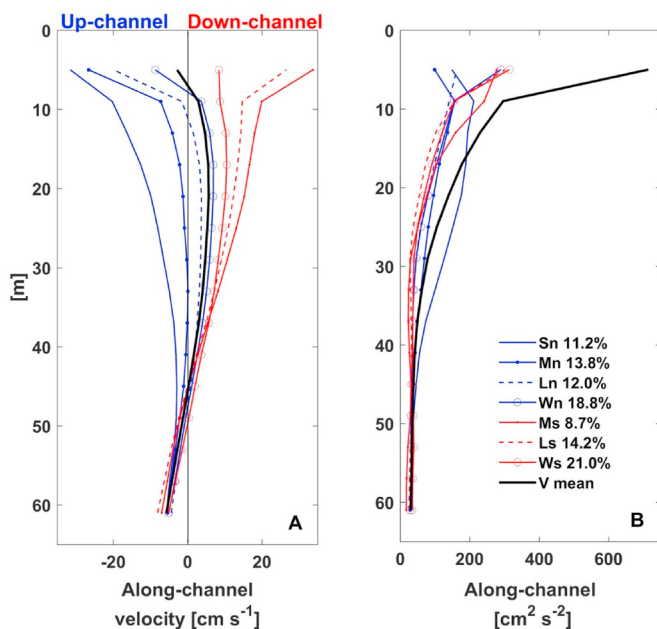


Fig. 8. a) Response of the monthly averaged residual current (ADCP) for each wind classification and the b) variance profiles. The legend labels indicate profiles for strong northward (Sn, $w \leq 0.06 \text{ N m}^2$), moderate northward (Mn, $0.06 < w < 0.03 \text{ N m}^2$), flow northward (Ln, $0.03 < w < 0.015 \text{ N m}^2$), weak northward (Wn, $0.015 < w < 0 \text{ N m}^2$), moderate southward (Ms, $0.03 < w < 0.06 \text{ N m}^2$), flow southward (Ls, $0.015 < w < 0.03 \text{ N m}^2$), weak southward (Ws, $0 < w < 0.015 \text{ N m}^2$) wind stress and the wind velocity mean (Vmean). Note that there were no instances of strong southward winds.

residual current was two-layer, indicating of gravitational circulation. The magnitude of the residual velocity in the upper 30 m of the water column increased proportionally with the magnitude of the wind stress. Under the influence of up-channel wind events, the residual flow is modified from the typical gravitational circulation vertical structure. With flow and weak wind stress, the residual flow vertical structure

becomes three-layer. The first layer is the upper 10 m of the water column where the current follows the up-channel wind. From 10 m to 40 m the current is dominated by gravitational circulation and is down-channel. Below 40 m depth, the residual flow is directed up-channel. The second type of structure produced by the up-channel wind events (moderate and strong wind) is unfixed to the south and these events are capable of erasing the gravitational circulation structure. The variance profile (Fig. 8b) shows a high variability over the upper 10 m decreasing with depth.

3.4. Stratification and mixing

Using the hydrodynamic model, the influence of wind and freshwater forcing on stratification and mixing was investigated over a full year (April 2018 to March 2019). The fall and winter months (April to September) is when there is the least amount of freshwater (<5%) in Moraleda Channel (Fig. 9a) and up-channel wind events of high intensity and magnitude dominate (Fig. 9b). Values of the Richardson number indicate a water column favorable for turbulent mixing from the surface to 30–35 m depth in the fall and winter ($R_i < 0.25$; Fig. 9c). The Brunt–Väisälä frequency was lowest during this season (Fig. 9d), as the surface salinity increased (Fig. 9e). Two months stand out with this described period; August and September when freshwater flows were lowest and wind stress was high. During these months flow Richardson numbers ($R_i < 0.25$) reached from the surface to 35 m and the 32 psu isohaline reached the surface, which is in line with the flow Brunt–Väisälä values ($N^2 < 2 \times 10^{-4} \text{ s}^{-2}$) and stratification parameter, n_s (<0.15). These conditions are favorable for turbulent mixing down to a depth of 35 m, which implies a high diffusion of freshwater.

In the spring and summer months (October to March), the percentage of freshwater increases (>10%) with a maximum between November and December (>15%). The intensity of up-channel wind events decreases, and down-channel wind events become more frequent with the maximum values of Richardson numbers ($R_i < 0.25$) in the upper 5–10 m of the water column. Elevated Brunt–Väisälä values ($N^2 > 4 \times 10^{-4} \text{ s}^{-2}$) in the upper 30 m of the water column, with salinity less than 30 psu at the surface (<10 m), and the stratification parameter n_s nearing 0.1 indicate enhanced stratification during several periods in the spring and summer.

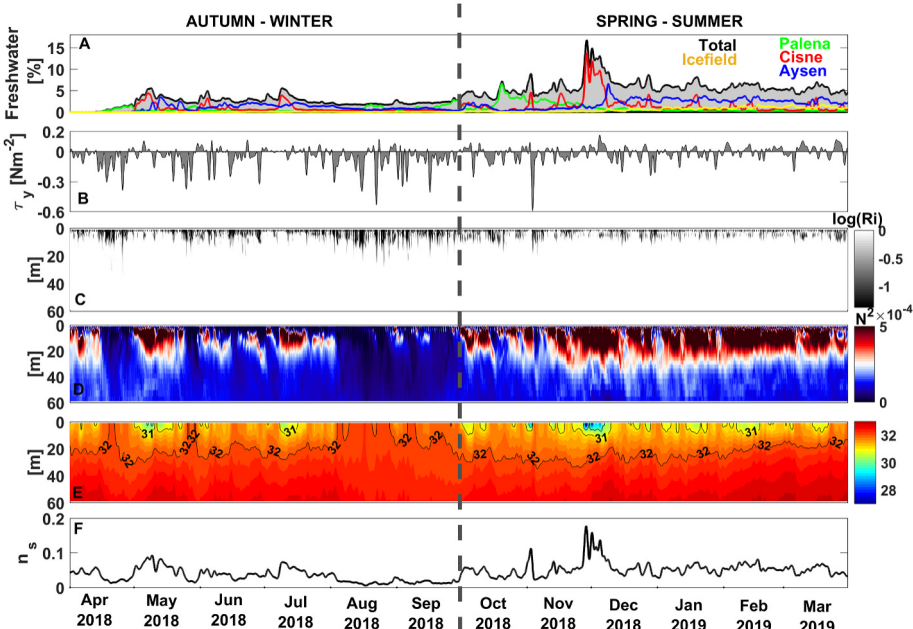


Fig. 9. Results from the hydrodynamic and climate model (WRF) showing a) the percentage of freshwater in the Moraleda Channel; b) wind stress along the channel (WRF); c) gradient Richardson number profiles; d) Brunt–Väisälä frequency; e) salinity and f) the stratification parameter (bottom = 60 m). The dashed line separates autumn/winter from spring/summer.

The extent of the influence of seasonal variations in stratification and wind forcing on residual flow vertical structure is now investigated.

3.5. Residual circulation during up-channel and down-channel wind events

An up-channel wind event occurred between the 16th and 26th of September 2018 (11 days). This event was compared with a down-channel wind event from November 27th to December 7th of 2018 (11 days) to assess the impact of wind forcing on residual circulation in Moraleda Channel (Fig. 10a). Model runs with and without wind forcing were analyzed for both events over the entire water column to extrapolate the information reflected by the ADCP (moored at 60 m depth). During the up-channel wind event (Fig. 10a), the freshwater percentage was <5% in Moraleda Channel (Fig. 10a1). When wind was included in the simulations, the along-channel residual currents show a two to three-layer vertical structure with an upper flow layer (southward), a lower outflow layer (northward), and a near-bottom (between 100 and 350 m depth) flow (southward) that occurs only when the wind stress is elevated ($\tau > 0.1 \text{ N/m}^2$; e.g., September 16–17 (Fig. 10a2 and a3)). The model without wind (Fig. 10a4) shows a clear two-layer vertical structure with out-channel (northward) current at the surface decreasing with depth and in-channel (southward) current at depth (between 80 and 350 m). The stratification parameter, n_s , from the model with wind showed values close to 0.005 while the stratification without wind was much higher ($n_s = 0.15$), indicating that wind weakened and even reversed the residual circulation (Fig. 10a5). The exchange flux was predominantly directed in-channel (southward) from September 19–26 (Fig. 10a6). In comparison, the model without wind was continually

stratified (n_s of 0.2), and there was a continuous out-channel (northward) exchange flux of 5 cm s^{-1} .

During a down-channel wind event (Fig. 10b), there is a greater percentage of freshwater in the Moraleda Channel (>15%). The along-channel residual current with wind now clearly displays a two-layer vertical structure, with velocities reaching 20 cm s^{-1} in the upper 20 m of the water column with strongest pulses of residual out-channel flow when wind stress values were down-channel (positive) and elevated (Fig. 10b2 and 3, e.g., December 6–8). The model simulation without wind also shows a two-layer along-channel residual flow structure that does not include the out-channel pulses of surface residual flow as wind is not included (Fig. 10b4). It should be noted that when wind was not included, the two-layer residual flow magnitude is larger for the down-channel wind case (Fig. 10b4) than the up-channel wind case (Fig. 10a4) due to the enhanced freshwater content in the channel during the months when down-channel wind events occur. This is also reflected in the stratification parameter, n_s , that was elevated (>0.2) in the model without wind (Fig. 10b5) more so during the down-channel wind event than the up-channel. However, in the model with wind, n_s reached a maximum of 0.2 on November 28th and overall was much larger than during the up-channel wind events. The exchange flux was continuous and positive to the north at 10 cm s^{-1} (Fig. 10b6). In comparison, the exchange flux was greater (18 cm s^{-1}) in the model with wind, confirming with the highest magnitude of wind stress on November 5th.

The spatial variability of the along-channel residual flow during up- and down-channel wind events is now investigated. During the up-channel wind event the along-channel velocity at the surface is directed up-channel on the eastern side and down-channel on the western side. The surface up-channel flow is stronger than the down-

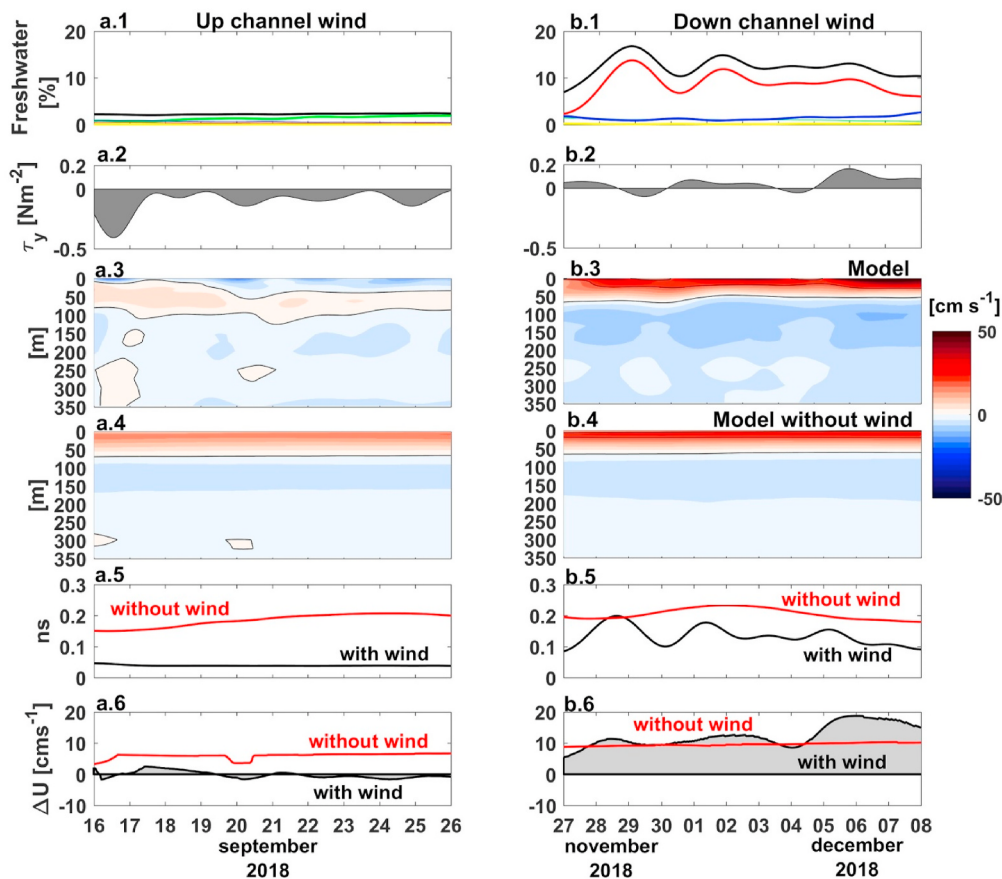


Fig. 10. a) Up-channel wind event, b) down-channel wind event. 1) Percentage of freshwater in the Moraleda Channel (Model); 2) wind stress along the channel (WRF); 3) residual current along the channel (model with wind); 4) residual current along the channel (model without wind); 5) stratification parameter (bottom = 350 m) and 6) exchange flux.

channel flow (Fig. 11b). The vertical structure of the along-channel residual flow is three-layer on the eastern side of the channel (Fig. 11a). The near-surface (upper 50 m) along-channel residual current on the eastern side of the channel follows the direction of the wind (southward). Below 50 m depth there is outflow (from ~50 m–100 m depth), and below 100 m depth there is inflow. On the western side of the channel the along-channel residual flow is two-layer. The near surface (upper ~100 m) along-channel residual flow is towards the north and below ~100 m the circulation is to the south with lower velocity than the near surface flow (<5 cm s⁻¹).

During a down-channel wind event, the along-channel residual flows at the surface are directed out-channel (to the north) in the upper ~50 m of the water column (>10 cm s⁻¹; Fig. 11c and d). Below ~50 m depth the along-channel velocity is up-channel, with strongest up-channel velocities in the center of the channel (average up-estuary velocity of 8 cm s⁻¹; Fig. 11c). The vertical structure of the wind-induced flow, wind down-wind flows near the surface and a return flow at depth, reinforces the gravitational circulation in the channel. The up and down-channel wind events indicate that the velocity response to the wind is not symmetrical, and thus can lead to non-zero mean flow patterns.

4. Discussion

This study aimed to elucidate the competition between residual circulation induced by freshwater input and by the wind. The spatial and temporal variation in the residual circulation structure was also investigated in relation to seasonal stratification conditions, and the potential for mixing in the Moraleda channel. A combination of *in-situ* reflected data and hydrodynamic model simulation output was used to study these processes. The hydrodynamic model used in this study is one of the most extensive models of Northern Patagonia to date. The results of this study will now be discussed in relation to other fjords in Chile and worldwide. The model and study limitations will also be mentioned.

4.1. Tide, river, and wind influence in the Moraleda Channel

The tide has been found to greatly influence the circulation of Patagonia's inland sea. Afken (2008) used a barotropic model of north Patagonia's inland sea to show that the most prominent feature is the significant increase in tidal amplitude that occurs with distance from the Boca del Guafo mouth both to the north and south. The amplification is largest towards the north of the Boca del Guafo, with amplitudes of the semidiurnal tides in Reloncaví Sound being up to a factor of 5 larger than on the Pacific coast. At the southern end of the Aysen inland sea tidal amplification is only a factor of approximately 2 larger than on Pacific coastal waters (Afken, 2008). In Moraleda Channel the semidiurnal and diurnal tidal harmonics explained 20% and 3% of the variance of the total current in the Moraleda Channel, respectively. This does not coincide with the findings of Pierri et al. (2000), who characterized the regime of tides and currents in the Moraleda and concluded that the variance associated with the tidal currents was between 42% and 65% of the total variance. This discrepancy could be due to the changes in depth associated with the proximity to the coast where the observations were taken close to Nassau Island and Puerto Bafle. In addition to tides, freshwater and wind forcing were found to be influential in the Moraleda Channel.

The greatest contributions of freshwater to the Moraleda Channel come from the Aysén (640 m³s⁻¹) and Cisnes (334 m³s⁻¹) Rivers, while the Pallen River (987 m³s⁻¹) and the Northern Icefield basin (795 m³s⁻¹), with the largest discharges, present less of an influence. The Pallen is the single largest contributor of freshwater, but the river mouth is located north of Moraleda channel entering directly into the Boca del Guafo. Freshwater from the Northern Icefields is likely mixed out of the surface layer in regions like the Menfina constriction/Siflif (Fig. 1).

The typical annual variability of freshwater input from the rivers has two maxima during winter and spring and one minimum in the summer. The freshwater content estimated by the model at the ADCP

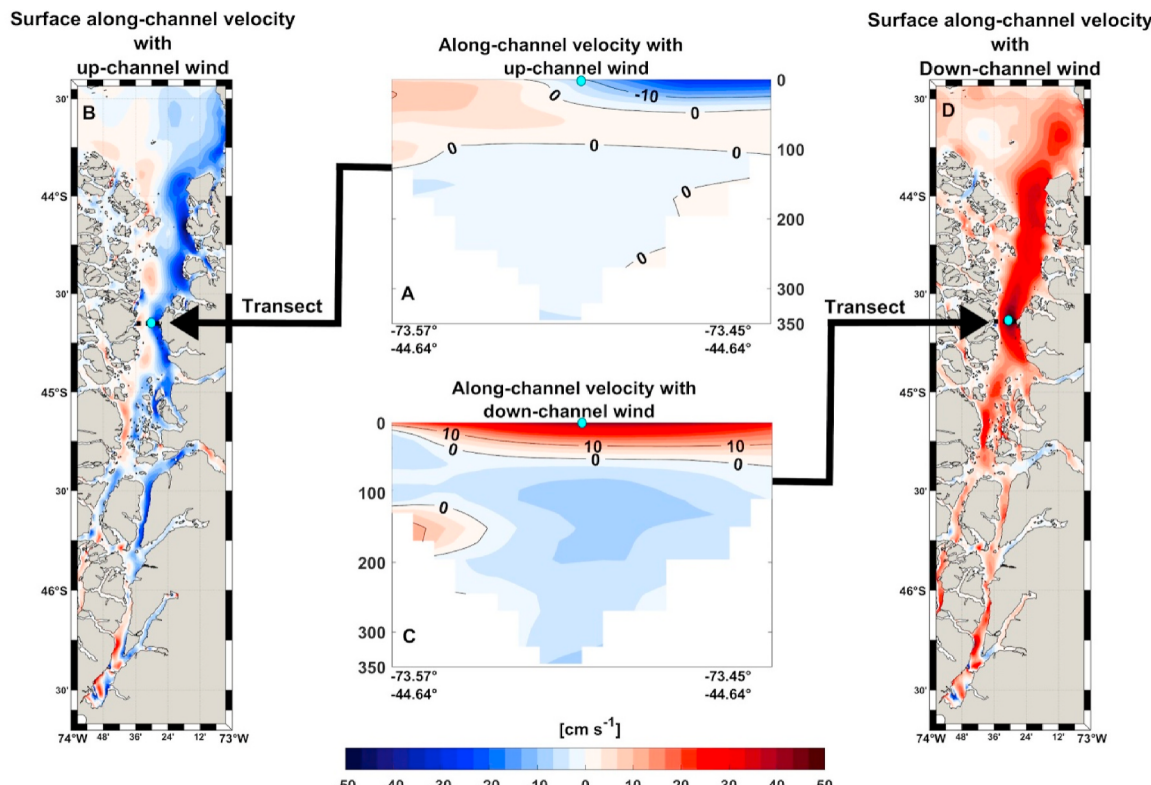


Fig. 11. Residual current from the numerical model (cyan circles indicate ADCP location). a) Along-channel residual velocity averaged over up-channel wind event, b) surface along-channel residual velocity averaged over up-channel wind event, c) Along-channel residual velocity averaged over down-channel wind event, d) surface along-channel residual velocity averaged over down-channel wind event.

mooring site showed two minimums (<5% freshwater contribution) in April and August–September. In April (early fall), the freshwater input was low, and the wind was moderate to low, directed predominantly to the south. In August–September (autumn and winter), freshwater input was high, but elevated wind to the south dominated and near surface mixing diluted the freshwater influence, a result consistent with Rufiz et al. (2021). The percentage of freshwater in Moraleda Channel was highest in November, which coincides with the maximum freshwater input from the rivers and moderate northward winds, which favor stratification in the water column. In contrast to the seasonal timescales of the variation in buoyancy, wind forcing was found to be highly variable over shorter time scales. Wind forcing has been found to be highly correlated with current velocities (Lange and Burchard, 2019) and the impact of wind forcing on residual flows will now be discussed.

4.2. Modification of residual flows by wind forcing

Results of this study indicated that freshwater input and wind are the two primary forcing mechanisms of residual circulation in the Moraleda Channel, with the extent of their influence varying depending on the season. In fall and winter months, up-channel wind dominates, enhancing mixing and reducing stratification. During these seasons, the wind can modify the estuarine circulation or reverse its direction. In spring and summer, the residual circulation is gravitational, which when coupled with a down-channel wind, maintains and enhances the gravitational circulation. Results suggest that the residual flows are significantly correlated with the wind stress along the channel. The correlation between wind stress and along-channel current velocities were found to reach 0.7 in the upper 30 m of the water column (Fig. 7e). Vaifile-Levinson et al. (2002) focused their study on understanding the estuarine exchange flow in a Patagonian Fjord with an emphasis on investigating the wind forcing. They concluded that the wind forcing can modify the typical two-layer circulation structure in fjords and asserted that up-fjord wind becomes a barrier to the exchange flow and down-fjord wind can enhance the two-layer exchange, however they were not able to confirm this result due to a lack of data. The results of this study were able to confirm the findings of Vaifile-Levinson et al. (2002) and go further to examine the seasonal and spatial extent of wind forcing in Patagonian fjords and channels.

Elevated up-channel winds made up ~25% of all wind directions and magnitudes considered in this study. These wind events caused the residual current in the upper water column to be directed up-channel, which weakened or halted the gravitational circulation (Fig. 8a). Weak up-channel winds produced a three-layer vertical residual flow structure, where the wind-driven residual currents were found from the surface to 10 m depth. In the case of down-channel wind, the two-layer estuarine structure is maintained, and the greater the magnitude of the wind stress, the greater the out-channel velocity of the surface layer. As mentioned by Vaifile-Levinson et al. (2014), fjord circulation is typically assumed to be driven by density forcing and be two-layer. However, they observed that a three-layer structure can be observed, and is driven by the tide in deep fjords, characterized by a water column depth that is six or more times greater than the depth of the gravitational influence. The Moraleda Channel is deep (>300 m), but tidal forcing was found to be weak (<20% of the total variability). A three-layer residual flow structure was observed however but is explained by wind forcing. The study by Vaifile-Levinson et al. (2014) found that the three-layer tidal-driven residual circulation structure could become masked by wind-driven flow.

The influence of wind on the residual currents in the Moraleda channel depend on the competition between wind direction and magnitude and freshwater input which enhances the baroclinic pressure gradient. Both the model and observations show transient episodes, in which the wind stress can provide momentum to the water column. This wind action can act in opposition to the baroclinic pressure gradient and modify the dynamics during these events (Farmer and Freehand, 1983;

Inglis and Giffibrand, 2010; Vaifile-Levinson et al., 2002). This was observed in the Jacaf channel, located adjacent to the Moraleda channel, in a study by Pfiffli et al. (2020).

In terms of wind aftereffect stratification in the Moraleda Channel, the results of this study are consistent with the regimes described in Perez-Santos et al. (2014) and Rufiz et al. (2021), who also found seasonal variability in the channel. In the partially mixed Chesapeake Bay, Scully et al. (2005) observed that wind forcing can act to strain the density gradient and control vertical stratification. Subsequently, Chen et al. (2009) and later Xie and Li (2018) studied wind effects on stratification in partially mixed estuaries. They found that the wind effect on estuarine stratification depends on if the wind direction and intensity allows for enhanced mixing or enhanced stratification. Both studies found that moderate down-channel winds enhance stratification, but strong down-channel directed winds and a up-channel directed winds reduce stratification. The results of this study in a fjord and channel system in Patagonia has shown that this same result can be found in highly stratified, deep estuaries. This effect could be found in other fjord systems due to the mountainous landscape funneling along-channel winds.

To generalize the seasonal variation in residual circulation patterns of the study in Moraleda Channel, a schematic diagram is presented and represents the residual flow throughout the water column during both up- and down-channel wind events (Fig. 12). In the fall and winter seasons the residual circulation has a 3-layer vertical structure due to wind blowing up-channel and counteracting the gravitational circulation pattern (Fig. 12a). The three-layer structure is found on the eastern side of the channel, whereas there is a two-layer vertical structure on the western side, indicating horizontal exchange flux in addition to vertical (Fig. 11a and b). These results are in agreement with the findings of Wan et al. (2022) who found that wind forcing can produce cross-channel variability in circulation patterns even in narrow fjords. During this scenario, the pycnocline is stretched as salt water is mixed with fresh surface water in the upper layer, causing the exchange flux to decrease. During the spring and summer seasons, the wind blows down-channel and the residual flow vertical structure is dominated by gravitational circulation and accentuated by the wind-driven outflow at the surface. This mixing, weakens mixing and elevates the exchange flux (Fig. 12b).

4.3. Study limitations

The hydrodynamic model evaluated in Moraleda channel was able to reproduce the two-layer estuarine circulation structure during spring and summer, when the south wind is less intense or blows north. However, the model has a lower capacity to reproduce the intensity of the current when strong winds blow to the south, mainly in winter. This may be due to several factors. For example, the WRF model does not adequately reproduce the intensity and direction of the wind in Moraleda channel. Although the WRF evaluation against data showed relatively good agreement at one point, there may be an increase in the error of the WRF model in the Moraleda channel. Another possibility is that the parameterization of the wind stress within the hydrodynamic model is not totally adequate to the conditions of the Moraleda channel. Finally, the representation of the horizontal density gradient could be overestimated, generating an inadequate balance. This would result in transient events of intense southward wind that influence the current to be underestimated by the model. Therefore, results from these periods must be taken with care. Overall the model does reproduce the process of changes in the flow structure, therefore, for the purposes of this study, the information from the model is deemed useful to help understand mixing and stratification processes as well as general residual circulation patterns.

One additional limitation is the limited depth of the ADCP measurements in Moraleda Channel. The channel is 368 m deep at the mooring location, yet the ADCP reflected data in the upper 60 m of the

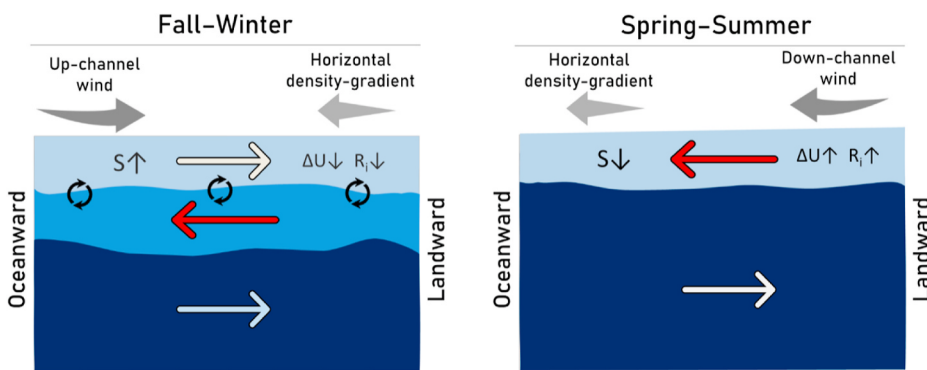


Fig. 12. Schematic representation of the residual circulation in the Moraleda channel for up-channel wind events and b) down-channel wind events. The arrows indicate the direction of the residual flow, S is salinity (represents the upper layer), ΔU is the exchange flux, R_i is the Richardson Number, and the black circular arrows indicate mixing.

water column due to mooring and instrument constraints. To the best of the author's knowledge there is no available observational data over the entire water column in Moraleda Channel. Therefore, the formation of the 3-layer vertical residual flow structure forced by the southward wind is from the numerical model at depths not validated with measurements. However, as there is evidence of the existence of 3-layer vertical residual flow structures in other channels and fjords of Patagonia (Vafle-Levinson et al., 2014), we believe our results represent a reasonable and likely finding in Moraleda Channel. It is recommended that future studies consider collecting measurements in the lower water column to confirm these results.

5. Conclusion

A combination of *in-situ* collected data and atmospheric and hydrodynamic models were used to understand the contribution of freshwater and wind forcing to residual circulation, stratification and exchange flux in a channel that connects part of northern Patagonia with the Pacific Ocean. Results showed that the along-channel residual flow in the Moraleda Channel is primarily gravitational, induced by the flow surface density from multiple rivers and glacial melt inputting freshwater into the fjord and channel system. The intensity of the gravitational circulation is seasonal and dependent on the wind intensity and direction. In spring and summer months' gravitational circulation dominates and is reinforced by dominant down-channel winds from the south favoring stratification. In the fall and winter seasons the gravitational circulation is modified by elevated up-channel winds, which diminishes and even reverses the exchange flux creating a three-layer vertical residual flow structure on the eastern side of the channel and a two layer structure on the western side. The increase in vertical shear of the current due to the wind influence increases mixing in the water column, which weakens the pycnocline. The seasonality of the channel is due to Moraleda's sensitivity to wind, which is explained by its north-south orientation and mountainous landscape that funnels winds in the axial direction.

Declaration of competing interest

The authors declare that they have no known competing financial interests or personal relationships that could have appeared to influence the work reported in this paper.

Acknowledgments

We thank the Ministry of Economy, Development and Tourism of the Chilean Government for funding through the Undersecretary of Fisheries and Aquaculture, and the Instituto de Fomento Pesquero (IFOP) for providing the high-performance computing system for ocean-atmospheric modeling. Lauren Ross would like to acknowledge

funding from the National Science Foundation (NSF) Grant Number 2045866 that partially contributed to the work presented in this study.

Appendix A. Supplementary data

Supplementary data to this article can be found online at <https://doi.org/10.1016/j.csr.2022.104905>.

References

Afken, C.M., 2008. Barotropic tides of the Chilean Inland Sea and their sensitivity to basin geometry. *J. Geophys. Res.: Oceans* 113 (C8).

Archfield, S., Vogel, R., 2010. Map correlation method: selection of a reference streamgage to estimate streamflow at ungaged catchments. *Water Resour. Res.* 46, W10513 <https://doi.org/10.1029/2009WR008481>.

Bendat, J., Piersol, A., 1986. *Random Data: Analysis and Measurement Procedures*. John Wiley, p. 566.

Cáceres, M., Vafle-Levinson, A., Sepúlveda, H., Hofstede, K., 2002a. Transverse variability of flow and density in a Chilean fjord. *Continent. Shelf Res.* 22, 1683–1698. [https://doi.org/10.1016/S0278-4343\(02\)00032-8](https://doi.org/10.1016/S0278-4343(02)00032-8).

Cafvete, C., Sobaro, M., 2011. Quantification of the surface brackish water layer and frontal zones in southern Chilean fjords between Boca del Guapo (43° 30' S) and Estero Elefante (46° 30' S). *Continent. Shelf Res.* 31, 162–171. <https://doi.org/10.1016/j.csr.2010.09.013>.

Carrasco, C., Siflva, N., 2010. Comparación de las características oceanográficas físicas y químicas presentes en la zona de Puerto Montt a la boca del Guapo entre el invierno y la primavera de 2004 y entre las primaveras de 1995 y 2004. *Cienc. Tecnol. del Mar* 33 (2), 17–44.

Cáceres, M., Vafle-Levinson, A., Sepúlveda, H., Hofstede, K., 2002b. Transverse variability of flow and density in a Chilean fjord. *Continent. Shelf Res.* 22, 1683–1698.

Castillo, M.I., Pizarro, O., Cifuentes, U., Ramírez, N., Djurfeldt, L., 2012. Subtidal dynamics in a deep fjord of southern Chile. *Continent. Shelf Res.* 49, 73–89.

Castillo, M.I., Cifuentes, U., Pizarro, O., Djurfeldt, L., Cáceres, M., 2016. Seasonal hydrography and surface outflow in a fjord with a deep sill: the Reloncaví fjord, Chile. *Ocean Sci.* 12 (2), 533–544.

Chen, S.-N., Sanford, L.P., Raflston, D.K., 2009. Lateral circulation and sediment transport driven by axial winds in an idealized, partially mixed estuary. *J. Geophys. Res.: Oceans* 114, C12006 <https://doi.org/10.1029/2008JC005014>.

Crawford, D.W., Montero, P., Daner, G., 2021. Blooms of *Alexandrium catenella* in coastal waters of Chilean Patagonia: is subantarctic surface water involved? *Front. Mar. Sci.* 8, 326. <https://doi.org/10.3389/fmars.2021.660326>.

Davis, K.A., Banas, N.S., Giddings, S.N., Siedlecki, S.A., MacCready, P., Lessard, E.J., Kudela, R.M., Hickey, B.M., 2014. Estuary-enhanced upwelling of marine nutrients fuels coastal productivity in the U.S. Pacific Northwest. *J. Geophys. Res.: Oceans* 119 (12), 8778–8799. <https://doi.org/10.1002/2014JC010248>.

Díaz, P., Pérez-Santos, I., Alvarez, G., Garreaud, R., Pinilla, E., Díaz, M., Sandoval, A., Araya, M., Alvarez, F., Rengel, J., Montero, P., Pizarro, G., López, L., Irarate, L., Igor, G., Reguera, B., 2021. Multiscale physical background to an exceptional harmful algal bloom of *Dinophysis acus* in a fjord system. *Sci. Total Environ.* 773, 145621 <https://doi.org/10.1016/j.scitotenv.2021.145621>.

DHI, 2016. Mike 3, User Guide and Reference Manual. Danish Hydraulic Institute, Denmark.

Emery, W.J., Thomson, R.E., 1998. *Data Analysis Methods in Physical Oceanography*. Pergamon Press, Oxford, p. 634.

Farmer, D.M., Freehand, H.J., 1983. The physical oceanography of fjords. *Prog. Oceanogr.* 12, 147–220.

Fierro, J., Bravo, M., Castelló, M., 2000. Characterization of the tidal regime and currents along the Moraleda Channel. *Cienc. Tecnol. Mar* 23, 3–14.

Geyer, W.R., Cannon, G.A., 1982. Shallow processes related to deep water renewal in a fjord. *J. Geophys. Res.* 87, 7985–7996.

Geyer, W.R., Farmer, D.M., 1989. Tidal induced variation of the dynamics of a salt wedge estuary. *J. Phys. Oceanogr.* 28, 1060–1072.

Geyer, W.R., 1997. Influence of wind on dynamics and flushing of shelfflow estuaries. *Estuar. Coast Shelf Sci.* 44, 713–722. <https://doi.org/10.1006/ecss.1996.0140>.

Geyer, W.R., MacCready, P., 2014. The estuarine circulation. *Annu. Rev. Fluid Mech.* 46, 175–197. <https://doi.org/10.1146/annurev-fluid-010313-141302>.

Giddings, S.N., MacCready, P., 2017. Reverse estuarine circulation due to local and remote wind forcing, enhanced by the presence of along-coast estuaries. *J. Geophys. Res.: Oceans* 122. <https://doi.org/10.1002/2016JC012479>, 10, 184–10, 205.

Guerra, D., Siflva, N., 2004. Distribución de temperatura, salinidad, oxígeno disuelto y nutrientes entre la boca del Guao y el fiordo Aysén. Resultados crucero CIMAR 9 Fiordos. *Comité Oceanográfico Nacional, Valparaíso 15–24. Libro de Resúmenes.*

Guzmán, L., Pacheco, H., Pízarro, G., Aflacón, C., 2002. Alegriaeum catenella y veneno paralizante de los mariscos en Chile. Flora y fauna marinas en el Cono Sur Americano 237–255.

Haralambidou, K., Syfalois, G., Tsiflakis, V.A., 2010. Salt-wedge propagation in a Mediterranean micro-tidal river mouth. *Estuar. Coast Shelf Sci.* 90 (4), 174–184. <https://doi.org/10.1016/j.ecss.2010.08.010>.

Inall, M.E., Griffiths, P.A., 2010. The Physics of Mid-latitude Fjords: A Review. *Geophysical Society, vol. 344. Publications, London, UK, Special, pp. 17–33.*

Lange, X., Burchard, H., 2019. The relative importance of wind straining and gravitational forcing in driving exchange flows in tidally energetic estuaries. *J. Phys. Oceanogr.* 49 (3), 723–736. <https://doi.org/10.1175/JPO-D-18-0014.1>.

Lange, X., Kelling, K., Burchard, H., 2020. Inversions of estuarine circulation are frequent in a weakly tidal estuary with variable wind forcing and seaward salinity fluctuations. *J. Geophys. Res.: Oceans* 125, e2019JC015789. <https://doi.org/10.1029/2019JC015789>.

Li, M., Zhong, L., Bofcourt, W.C., Zhang, S.L., Zhang, D.L., 2007. Hurricane-induced destratification and restratification in a partially mixed estuary. *J. Mar. Res.* 65 (2), 169–192. <https://doi.org/10.1357/002224007780882550>.

Large, W.G., Pond, S., 1981. Open-ocean momentum flux measurements in moderate to strong winds. *J. Phys. Oceanogr.* 11, 324–336.

Li, Y., Li, M., 2011. Effects of winds on stratification and circulation in a partially mixed estuary. *J. Geophys. Res.* 116, C12012 <https://doi.org/10.1029/2010JC006893>.

Mardones, J.I., Clement, A., Rojas, X., Aparicio, C., 2010. Alegriaeum catenella during 2009 in Chilean waters, and recent expansion to coastal ocean. *Harmful Algae Newsletter* 41, 8–9.

Mardones, J.I., Paredes, J., Godoy, M., Suárez, R., Norambuena, L., Vargas, V., Fuenzaflida, G., Píñar, E., Artafl, O., Rojas, X., Dorantes-Aranda, J.J., Lee Chang, K.J., Anderson, D.M., Hasslegrave, G.M., 2021. Disentangling the environmental processes responsible for the world's largest farmed fish in the harmful algal bloom: Chile. *Sci. Total Environ.* 766, 144383 <https://doi.org/10.1016/j.scitotenv.2020.144383>.

Muñoz, P., Avaria, S., Sfevers, H., Prado, R., 1992. Presencia de dinoflagelados tóxicos del género en el Seno Aysén, Chile. *Revista de Biología Marinha e Estuários* 27, 187–212.

Narváez, D.A., Vargas, C.A., Cuevas, L.A., García-Loyola, S.A., Lara, C., Segura, C., Tapia, F.J., Broftman, B.R., 2019. Dominant scales of subtidal variability in coastal hydrography of the Northern Chilean Patagonia. *J. Mar. Syst.* 193, 59–73.

National Center for Environmental Prediction, 2000. NCEP FNL Operational Model Global Tropospheric Analyses, Continuing from July 1999. National Weather Service, U.S. Department of Commerce, Research Data Archive at the National Center for Atmospheric Research, Computational and Information Systems Laboratory, Boulder, CO.

Pérez-Santos, I., Garcés-Vargas, J., Schneidler, W., Ross, L., Parra, S., Vafle-Levinston, A., 2014. Double-diffusive layering and mixing in Patagonian fjords. *Prog. Oceanogr.* 129, 35–49. <https://doi.org/10.1016/j.pocean.2014.03.012>.

Pérez-Santos, I., Castro, L., Ross, L., Niflidsche, E., Mayorga, N., Cubillos, L., Gutiérrez, Escalona, E., Castelló, M., Alegria, N., Daner, G., 2018. Turbulence and hypoxia contribute to dense biological scattering layers in a Patagonian fjord system. *Ocean Sci.* 14 (5), 1185–1206.

Pérez-Santos, I., Seguel, R., Schneidler, W., Linford, P., Donoso, D., Navarro, E., Amaya-Cárcamo, C., Píñar, E., Daner, G., 2019. Synoptic-scale variability of surface winds and ocean response to atmospheric forcing in the eastern austral Pacific Ocean. *Ocean Sci.* 15, 1247–1266. <https://doi.org/10.5194/os-15-1247-2019>.

Píñar, E., Soto, G., Arrigada, M., Cañón, H., 2012. Difusión y estudio técnico de macrozonas de agrupaciones de coníferas en la zona sur austral X a XII Regiones. Valparaíso, Instituto de Fomento Pesquero Availble: http://190.151.20.106/exflibris/aleph/a23.1/apache_media/VB3VMRJKVR6S2C2I2E1XGA85FQPPC.pdf.

Píñar, E., Soto, G., Soto-Riquefime, C., 2019. Determinación de las escasas de intercambio de agua en fiordos y canales de la Patagonia, Etapa II. Valparaíso, Instituto de Fomento Pesquero. Availble: http://190.151.20.106/exflibris/aleph/a23.1/apache_media/K1E7N4VFQQ8B3Y8Y4I5NU9MSNA2QMD.pdf.

Píñar, E., Castelló, M.I., Pérez-Santos, I., Venegas, O., Vafle-Levinston, A., 2020. Water age variability in a Patagonian fjord. *J. Mar. Syst.* 210, 103376 <https://doi.org/10.1016/j.jmarsys.2020.103376>.

Pízarro, G., Paz, B., Aflacón, C., Toro, C., Frangópulos, M., Saflago, P., Orlave, C., Zamora, C., Pacheco, H., Guzmán, L., 2018. Wind distribution of toxic, potentialfly toxic phytoplankton, and shellfish toxins in fjords and channels of the Aysén region, Chile. *Lat. Am. J. Aquat. Res.* 46 <https://doi.org/10.3856/vof46-fissuel-fufltext-13>, 120–13.

Pritchard, D.W., 1954. A study of the salt balance in a coastal plume estuary. *J. Mar. Res.* 13, 133–144.

Pritchard, D., Viefira, M.E.C., 1984. Vertical variations in residual current response to meteorological forcing in the mid-Chesapeake Bay. In: *The Estuary as a Filter*. Academic Press, Orlando, pp. 27–65. <https://doi.org/10.1016/B978-0-12-405070-9.50009-8>.

Pawlowsky, R., Beardsley, B., Lentz, S., 2002. Classical tidal harmonic analysis including error estimates in MATLAB using T_TIDE. *Comput. Geosci.* 28, 929–937. [https://doi.org/10.1016/S0098-3009\(02\)00013-4](https://doi.org/10.1016/S0098-3009(02)00013-4).

Quinones, R.A., Fuentes, M., Montes, R.M., Soto, D., Leon-Munoz, J., 2019. Environmental issues in Chilean salmon farming: a review. *Rev. Aquacult.* 11 (2), 403–421. <https://doi.org/10.1111/raq.12337>.

Reche, P., Artafl, O., Píñar, E., Rufiz, C., Venegas, O., Arrigada, A., Fafley, M., 2021. CHONOS: oceanographic information website for Chilean Patagonia. *Ocean Coast Manag.* 208, 105634 <https://doi.org/10.1016/j.jocecoaman.2021.105634>.

Ross, L., Vafle-Levinston, A., Pérez-Santos, I., Tapia, F.J., Schneidler, W., 2015. Baroclinic annual variability of internal motions in a Patagonian fjord. *J. Geophys. Res. Oceans* 120, 5668–5685. <https://doi.org/10.1002/2014JC010669>.

Rodríguez, W., 1984. In: *Turbulence Models and Their Application in Hydraulics*. Delft, p. 104.

Ross, L., de Swart, H., Ensing, E., Vafle-Levinston, A., 2017. Three-dimensional tidal flow in a fjord-like basin with converging width: an analytical model. *J. Geophys. Res. Oceans* 122, 7558–7577. <https://doi.org/10.1002/2017JC012820>.

Ross, L., Huguenard, K., Sotolichio, A., 2019. Intratidal and fortnightly variability of vertical mixing in a macrotidal estuary: the Gironde. *J. Geophys. Res.: Oceans* 124 (4), 2641–2659. <https://doi.org/10.1029/2018JC014456>.

Rufiz, C., Artafl, O., Píñar, E., Sepúlveda, H.H., 2021. Stratification and mixing in the Chilean Inland Sea using an operational model. *Ocean Model.* 158, 101750 <https://doi.org/10.1016/j.ocemod.2020.101750>.

Saflinas, S., Castelló, M.I., 2012. Corrientes marinas y submareales en el Canal Desderores (421420 S, 0721500 W). *Ciencia y Tecnología del Mar* 35 (1), 10–17.

Schneidler, W., Pérez-Santos, I., Ross, L., Bravo, L., Seguel, R., Hernández, F., 2014. On the hydrography of Puyuhuapi channel, Chilean Patagonia. *Prog. Oceanogr.* 129, 8–18. <https://doi.org/10.1016/j.pocean.2014.03.007>.

Scuffell, M.E., Frerichs, C., Brubaker, J., 2005. Control of estuarine stratification and mixing by wind-induced straining of the estuarine density field. *Estuaries* 28 (3), 321–326. <https://doi.org/10.2307/3526916>.

Shan, S., Hannah, C.G., Wu, Y., 2019. Coupling of estuarine circulation in a network of fjords. *J. Geophys. Res.: Oceans* 124. https://doi.org/10.1029/2018JC014924809_830.

Siflva, N., Sfevers, H., Prado, R., 1995. Descripción oceanográfica de los canales australes de Chile. Zona Puerto Montt-Laguna San Rafael (Cruce Clímar-Fjordo 1). *Revista de Biología Marina y Estuaries* 30 (2), 207–254.

Siflva, N., Caflve, C., Sfevers, H., 1997. Características oceanográficas físicas y químicas de canales australes chilenos entre Puerto Montt y Laguna San Rafael (Cruce Clímar-Fjordo 1). *Cienc. Tecnol. del Mar* 20, 23–106.

Siflva, N., Caflve, C., Sfevers, H., 1998. Masas de agua y circulación para algunos canales australes entre Puerto Montt y Laguna San Rafael, Chile (Cruce Clímar- Fjordo 1). *Cienc. Tecnol. del Mar* 21, 17–48.

Skamarock, W.C., Klemp, J.B., Dudhia, J., Gill, D.O., Barker, D.M., Duda, M.G., Huang, X.-Y., Wang, W., Powers, J.G., 2008. A description of the advanced research WRF version 3. *NCAR Technical Note* 475, 125.

Soto, G., Píñar, E., Arrigada, M., Venegas, O., Saflas, P., 2017. Modelación de alta resolución aplicada al transporte hidrodinámico al interior del Estero Elefante XI Región de Aysén. Valparaíso, Instituto de Fomento Pesquero. Availble: <http://www.tifop.cl/wp-content/contenidos/uploads/Repositorio/flop/InformeFinal/P-656087.pdf>.

Stigebrandt, A., 1981. A mechanism governing the estuarine circulation in deep, strongly stratified fjords. *Estuarine, Coastal and Shelf Science* 13, 197–211.

Sutherland, D.A., Strange, R.S., 2014. Picard characteristics and dynamics of two major Greenland glacial fjords. *J. Geophys. Res.: Oceans* 119 (6), 3767–3791.

Thomson, R.E., Emery, W.J., 2014. Data Analysis Methods in Physical Oceanography. Elsevier, Waltham, Mass. Paperback, ISBN 9780123877826.

Turner, J.S., 1979. Buoyancy Effects in Flows. Cambridge University Press.

Vafdenegro, A., Siflva, N., 2003. Caracterización oceanográfica física y química de la zona de canales y fiordos australes de Chile entre el estrecho de Magallanes y cabo de Hornos (CIMAR 3 fiordo). *Cienc. Tecnol. del Mar* 26 (2), 19–60.

Vafle-Levinston, A., Blasco, J., Fierro, J.J., 2004. Observations of wind influence on exchange flows in a strait of the Chilean Inland Sea. *J. Mar. Res.* 62, 721–741.

Vafle-Levinston, A., Blasco, J.L., Fierro, J.J., 2002. Observations of wind effects on exchange flows in a channel constriction of the Chilean Inland Sea. In: *The Second Meeting on the Physical Oceanography of Sea Straits*, Viflaflefranche, vol. 15, pp. 223–227.

Vafle-Levinston, A., Sarkar, N., Sanay, R., Soto, D., Leon, J., 2007. Spatial structure of hydrography and flow in a Chilean Fjord. *Estuarine, Coastal and Shelf Science* 30 (1), 113–126.

Vafle-Levinston, A., Cáceres, M., Pízarro, O., 2014. Variations of tidal driven three layer residual circulation in fjords. *Ocean Dynam.* 64, 459–469.

Wan, D., Hannah, C.G., Foreman, M.G.G., Dosso, S., 2017. Subtidal circulation in a deep fjord: Douglas channel, British Columbia. *J. Geophys. Res. Oceans* 122, 4163–4182. <https://doi.org/10.1002/2016JC012022>.

Wan, D., Hannah, C.G., Cummings, P.F., Foreman, M.G., Dosso, S.E., 2022. Wind-driven currents in a "wedge" narrow channel, with application to Douglas channel, BC.

J. Geophys. Res.: Oceans 127 (8), e2021JC017887. <https://doi.org/10.1029/2021JC017887>.

Wefisberg, R.H., Sturges, W., 1976. Velocity observations in the west passage of Narragansett Bay: a partially mixed estuary. *J. Phys. Oceanogr.* 6 (3), 345–354.

Wong, K.-C., Lu, X., 1994. Low-frequency variability in Delaware's inland bays. *J. Geophys. Res.* 99 (C6), 12683–12695. <https://doi.org/10.1029/94JC00569>.

Xie, X., Li, M., 2018. Effects of wind straining on estuarine stratification: a combined observational and modeling study. *J. Geophys. Res.: Oceans* 123, 2363–2380. <https://doi.org/10.1002/2017JC013470>.

Lucas, L. (2010). Implications of estuarine transport for water quality.

Stewart, R. H.: Introduction to physical oceanography, Spring 2002 edn., Department of Oceanography, Texas A and M University, 350 pp., 2002.

Smagorinsky, J., 1963. General circulation experiments with the primitive equations. *Month. Weather Rev.* 91, 99–164. [https://doi.org/10.1175/1520-0493\(1963\)091<099:GCEWTP>2.3.CO;2](https://doi.org/10.1175/1520-0493(1963)091<099:GCEWTP>2.3.CO;2).

Wright, C.J., Ackleson, S.G., Davids, R.E., Fedde, J.J., Kifl, K.M., Legates, D.R., O'Donnell, J., Rowe, C.M., 1985. Statistics for the evaluation of model performance. *J. Geophys. Res.* 90 (C5), 8995–9005.